Sonolytic Design of Graphene–Au Nanocomposites. Simultaneous and Sequential Reduction of Graphene Oxide and Au(III)

ARTICLE *in* JOURNAL OF PHYSICAL CHEMISTRY LETTERS · JUNE 2010

Impact Factor: 7.46 · DOI: 10.1021/jz1006093

6 AUTHORS, INCLUDING:

Bernaurdshaw Neppolian
SRM University
70 PUBLICATIONS **2,634** CITATIONS
SEE PROFILE

Ian V Lightcap
University of Notre Dame
14 PUBLICATIONS **1,317** CITATIONS
SEE PROFILE

Prashant Kamat
University of Notre Dame
538 PUBLICATIONS **44,305** CITATIONS
SEE PROFILE

THE JOURNAL OF PHYSICAL CHEMISTRY Letters

pubs.acs.org/JPCL

Sonolytic Design of Graphene–Au Nanocomposites. Simultaneous and Sequential Reduction of Graphene Oxide and Au(III)

K. Vinodgopal,*,† B. Neppolian,‡ Ian V. Lightcap,§ Franz Grieser,‡ Muthupandian Ashokkumar,*,‡ and Prashant V. Kamat§

†Department of Chemistry, Indiana University Northwest, Gary, Indiana 46408, ‡School of Chemistry, University of Melbourne, Parkville, Victoria, Australia, and §Radiation Laboratory, Department of Chemistry & Biochemistry, University of Notre Dame, Notre Dame, Indiana 46556

ABSTRACT High-frequency ultrasound at 211 kHz is effective in developing graphene-based nanoarchitectures. Both simultaneous and sequential reduction steps have been employed to reduce the graphene oxide (GO) and a gold precursor, $HAuCl_4$. Characterization of the composites by transmission electron microscopy following the reduction process revealed well-dispersed Au nanoparticles on the reduced GO (RGO) sheets that are no more than a few layers thick (1–4 layers). The Raman spectra of the RGO–Au composites showed a distinct surface enhancement of the graphene Raman bands upon increasing the surface coverage of gold nanoparticles. The merits of sonolytic reduction in developing graphene-based composites are discussed.

SECTION Nanoparticles and Nanostructures

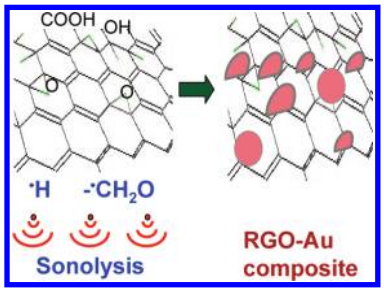

Catalyst assemblies based on metal and semiconductor nanoparticles deposited on exfoliated or single-layer graphene sheets show considerable promise in a variety of applications ranging from fuel cells to sensors[1−5] and capacitors to storage batteries.[6−10] Deposition of catalyst particles on graphene sheets not only allows large surface area but also assists in keeping the individual sheets well separated (Scheme 1).[11] The potential of these catalyst arrangements is based on the unique physical properties of the two-dimensional exfoliated graphene sheets, which include extremely large surface areas, high carrier mobility, mechanical strength, and so forth. The challenges in harnessing these potential advantages of graphene involve (i) the difficulty in maintaining exfoliated yet chemically reduced graphene sheets in solution matrices and (ii) ensuring wide uniform dispersal of catalyst particles on the sheets.

A variety of methods have been used to obtain graphene or reduced graphene oxide (RGO) dispersions in solution by reduction of the precursor graphene oxide (GO) solutions using reagents such as hydrazine and sodium borohydride and photocatalysts such as TiO_2 and ZnO.[3,7,12−16] Electrochemical and thermal methods provide direct reduction of graphene oxide films on electrode surfaces.[17,18] These reactions typically involve the reduction of the functional groups such as epoxides on the surface of GO, and the resulting suspensions of the RGO are more graphitic and conductive. Complete reduction of GO to restore the sp^2 graphite structure leads to unstable suspensions. Problems have been reported with hydrazine reduction arising from adsorption of the hydrazine to the graphene and delamination of graphene films when deposited on electrodes.[13] The challenge therefore is to use mild reduction conditions with minimal external reagents, which can give stable suspensions of the RGO. To this end, we have used sonochemistry to produce metal nanoparticles dispersed on RGO layers beginning with metal salt precursors and GO. The sonochemical reduction processes and dispersion of exfoliated RGO sheets are typically carried out at 20 kHz using a titanium horn, where the shear forces generated by the acoustic cavitation[19] are enough to overcome the van der Waals forces between the graphene sheets and prevent their reaggregation.[20]

The cavitation effects during sonolysis generate oxidative and reductive radicals that can be tuned to initiate specific chemical reactions.[21−25] A number of groups have shown over the years that sonication at frequencies ranging from 20 to 1000 kHz under reducing conditions can produce metal nanoparticles from aqueous solutions of metal salt precursors in the presence of surfactants.[26−34] In recent years, ultrasound-induced reduction of metal ions has been used to produce bimetallic nanoparticles with core–shell morphology.[33,35,36] The optimum ultrasound frequency for reduction has been determined to be around 200 kHz.[30,37,38] Sonication at this frequency provides higher radical concentrations conducive to faster chemical reductions.[19,39]

Received Date: May 11, 2010
Accepted Date: June 8, 2010
Published on Web Date: June 14, 2010

DOI: 10.1021/jz1006093 | J. Phys. Chem. Lett. 2010, 1, 1987–1993

Scheme 1. Dispersion of Graphene Sheets by Anchoring Metal Nanoparticles

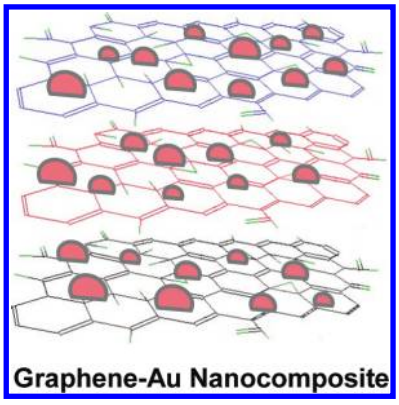

High-frequency ultrasound (HF-US) reduction of GO in the presence of metal ions can achieve the dual goals of a stable graphene suspension and wide dispersal of catalyst particles on the graphene surfaces. The question arises whether high-frequency ultrasound reduction can be used to tailor catalyst assemblies of metal nanoparticles dispersed on exfoliated reduced graphene oxide sheets. As compared to other chemical reduction methods, HF-US offers the advantages of no external chemical reagent and the ability to simultaneously reduce metal nanoparticles, offering potentially better dispersion over exfoliated graphene sheets.

We report here the ultrasound-induced reduction of graphene oxide in a 2 % aqueous solution of poly(ethylene glycol) (PEG) at an ultrasonic frequency of 211 kHz. The usefulness of sequential and simultaneous reduction in obtaining gold nanoparticle dispersion on RGO is discussed.

RGO and RGO–Au Nanocomposites. The interaction between ultrasound and dispersed monatomic (Ar) or diatomic (O_2, N_2) gas nuclei in aqueous solution results in acoustic cavitation, the growth and violent collapse of microbubbles. The near-adiabatic collapse of the cavitation bubbles leads to the generation of high-temperature conditions within bubbles. In aqueous solutions, highly reactive $H^\bullet$ and $OH^\bullet$ radicals are generated within the bubbles by the homolysis of water molecules due to the high-temperature conditions.[19,22−25,39−41]

$$H_2O \rightarrow H^\bullet + OH^\bullet \quad (1)$$

The reducing radicals ($H^\bullet$) have lesser probability of reacting with the target substrate in bulk solution. Henglein and co-workers[42] have shown that the majority of the H atoms produced within the cavitation bubbles do not reach the liquid phase. This is due to rapid H-atom recombination at the bubble−solution interface and the reaction $H + H_2O$ within the pyrolytic conditions of the cavitation bubbles.[43] This rules out the possibility of direct hydrogenation of GO to produce graphane.

The oxidizing radicals are scavenged by added organic solutes such as alcohols (reaction 2), surfactants, or poly(ethylene glycol) (PEG), thus providing a reducing condition. $H^\bullet$ can abstract a H from either the alpha hydrogen ($-CH_2$) or from $-OCH_2$ in the chain

$$R-(OCH_2CH_2O)_n-CH_2-OH + H^\bullet \rightarrow R-(OCH_2CH^\bullet O)_n - CH_2OH + H_2 \quad (2)$$

In addition, if the organic solutes are volatile, reducing radicals (e.g., $R-(OCH_2CH^\bullet O)_n-CH_2OH$, $R^\bullet$, etc.) are directly generated by the pyrolysis of the solutes within the bubbles. The organic radicals that are produced can subsequently reduce the target substrate, whether it be metal ions in solution, a suspension of GO, or a mixture of both metal ions and GO. The exact mechanism after the homolysis of water (reaction 1) leading to sonochemical reduction of a solute in aqueous solution containing solutes has been discussed elsewhere.[19,44,45] High-frequency sonication of an aqueous suspension of GO containing 2 % PEG (saturated with Ar) for 3 h produces a stable suspension of the RGO. Figure 1A shows the absorption spectra of graphene oxide recorded during ultrasound reduction. The broad absorption increases in intensity, consistent with the reduction of GO.

For the synthesis of the composites, we have employed two separate procedures consisting of simultaneous and sequential reduction of GO and Au(III). In the case of simultaneous reduction, tetrachloroauric acid (Au(III)) was mixed with the GO suspension and sonicated for at least 5 h to ensure that both the GO and the gold salt were reduced (reaction 3).

$$Au(III) + GO + \text{reducing species } (H^\bullet, R-(OCH_2CH^\bullet O)_n - CH_2OH, \text{etc.}) \rightarrow Au(0) + RGO \quad (3)$$

In the sequential reduction procedure, the GO was reduced first, and at the end of 3 h, $HAuCl_4$(or $AuCl_4^-$) solution was added and the sonication continued for another 2 h. In each case, the reduction of the metal ions was rapid, as is evidenced by the appearance of the gold surface plasmon band at 530 nm. In the sequential case, complete reduction of the gold occurs within 1 h of addition of the 0.1 mM Au(III) solution to the RGO suspension (Figure 1B). When the $HAuCl_4$ is sonicated simultaneously with the GO, reduction of the entire mixture is accomplished within four hours (Figure 1C). The position of the gold plasmon absorption band is also unchanged between the two reduction methods, indicating that particle sizes are comparable without any aggregation effects. In fact, graphene oxide has been used as a stabilizer during reduction of metal nanoparticles.[11,46]

We have employed the gold plasmon absorption band at 530 nm to follow the formation of gold nanoparticles. With continued sonolysis, we expect the 530 nm absorption to increase as more gold nanoparticles are formed in GO/RGO suspension. It should be noted that the reduction of GO to RGO also results in the absorption. The contribution of RGO to overall absorption is relatively small, as evidenced in the trace of sequential reduction. Figure 2 compares the reduction rates of the $HAuCl_4$ in GO suspension using both the simultaneous and sequential reduction methods. The reduction rate in the absence of GO (curve a), but at same concentration levels of 0.1 mM $HAuCl_4$ solution and 2 % PEG, shows a faster reduction with saturation in the absorption in ~30 min. A similar reduction rate for the $AuCl_4^-$ is also seen in the sequential reduction (curve c). The rate of reduction for the simultaneous

DOI: 10.1021/jz1006093 | J. Phys. Chem. Lett. 2010, 1, 1987–1993

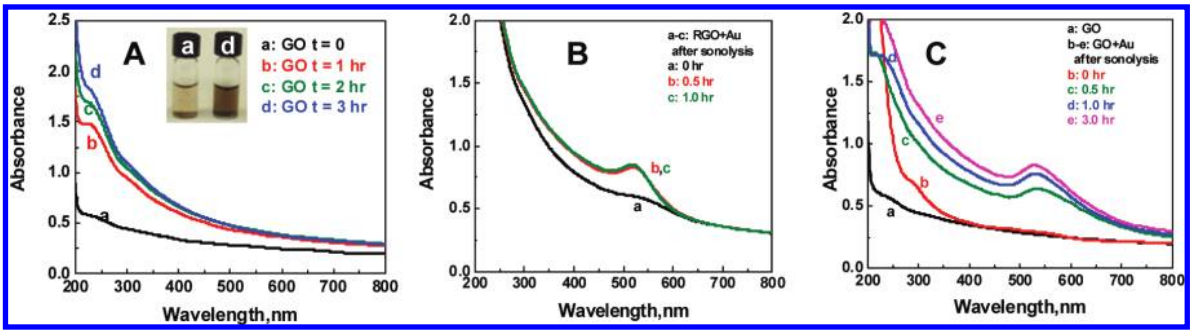

Figure 1. (A) Absorption spectra of 0.02% w/w GO in 2% PEG solution, recorded as a function of sonication times. Sonication was carried out at a frequency of 211 kHz in argon atmosphere. The inset photograph displays GO dispersions before and after sonication for 3 h. (B) Absorption spectra of 0.1 mM gold nanoparticles recorded as a function of sonication time in a sequential reduction process where the 0.1 mM $HAuCl_4$ was added to RGO. The RGO was obtained by ultrasound reduction of the GO for 3 h. (C) Absorption spectra of 0.1 mM gold nanoparticles recorded as a function of sonication time where the 0.1 mM $HAuCl_4$ was mixed with the 0.02% w/w GO in 2% PEG solution and the mixture was sonicated together for 4 h.

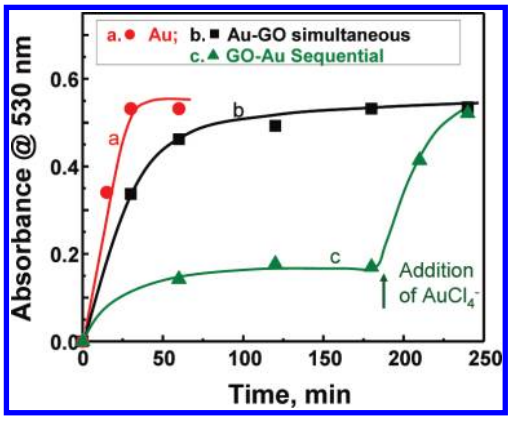

Figure 2. Relative reduction of the $HAuCl_4$ as monitored from the gold plasmon absorption band at 550 nm as a function with time of sonolysis. (a) Sonolytic reduction of a 0.1 mM $HAuCl_4$ solution in 2% PEG; (b) simultaneous reduction of the GO and $HAuCl_4$ in 2% PEG suspension; and (c) sequential sonolysis involving reduction of the GO for 180 min, followed by the addition of Au salt to the reduced GO suspension and continued sonolysis for an additional 60 min.

sonolysis experiment (curve b) is nearly 2.5 times slower with the completion of reduction of both GO and Au(III) in about 75 min. These results reflect the competition between the RGO and the Au (III) to seek reducing species during sonolysis.

The similarity in reduction rates between the $AuCl_4^-$ control and the sequentially reduced sample suggests that the presence of RGO does not affect the formation of Au nanoparticles. The results parallel an earlier observation made from transient absorption spectroscopy measurements of Au–RGO composites that the RGO merely serves as a 2-D support without directly influencing the optical properties of Au nanoparticles.[12] It is also interesting to note that the net increase in the 530 nm absorption at the end of 250 min is similar irrespective of the sonolytic procedure employed for the reduction of GO and $HAuCl_4$. The obvious question is whether the two sonolytic procedures provide any changes in the morphology.

Characterization of RGO. The extent of GO reduction has been determined by Raman spectroscopy, using both 514.5 and 785 nm laser excitation. Figure 3 shows the Raman spectra of the GO on a silicon wafer before and after high-frequency sonolytic reduction, with panels A and B corresponding to 514.5 and 785 nm excitation, respectively. In the case of the 514 nm excitation, we observe the expected increase in the D band at 1350 cm^{-1} relative to the G band at 1600 cm^{-1}.[17] Excitation at 785 nm also produces Raman spectra of the RGO with the expected increase in the D/G intensity ratios. However, the change in the D/G ratios and the changes in the absorption spectra do suggest partial reduction of the GO. The D/G ratio identifies the sp^2/sp^3 ratio and the density of defects. Although the absorption spectrum shows an increase in the graphitic sp^2 region, it fails to provide information on the defect sites. Hence, it is possible that the sonication process is producing defects as well as restoring graphitic structure. The inset from Figure 3 in the case of the 514 nm excitation shows the image from the Raman microscope (50× magnification) used to sample the Raman spectra. Edges corresponding to sheets that are three layers thick and that have more than a 20 μm lateral width are clearly visible.

Characterization of RGO–Au Composites. Jasuja et al. have shown that GO can serve as very effective anchors for metal nanoparticles.[47] This is likely due to the presence of oxygenated functional groups on the GO surface, which serve as nucleation and binding sites for the Au particles. One of the expected advantages of ultrasound reduction methods is that the gold nanoparticles should be well-dispersed on the surface of the exfoliated graphene sheets. The TEM images of the Au–RGO composites shown in Figure 4 present evidence of such dispersion. The images were obtained by drop casting samples of the composites on a holey carbon grid. At low resolution, the TEM images of both the sequential and simultaneous composite samples (panels A and B, respectively) reveal different dispersity of the metal particles on the RGO sheets. The sequential reduction steps produce smaller size particles, and they tend to exist as clusters on the graphene support. If the epoxide sites are first reduced, it is likely to prevent direct binding of $AuCl_4^-$ ions to the graphene sheets.

The simultaneous reduction on the other hand produces relatively well-dispersed but larger size particles. In the case of

DOI: 10.1021/jz1006093 | J. Phys. Chem. Lett. 2010, 1, 1987–1993

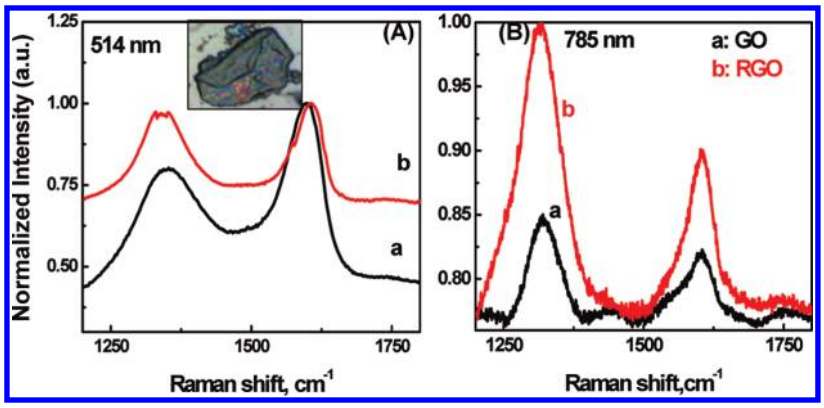

Figure 3. Raman spectra of GO (a) before and (b) after reduction using HF ultrasound for 3 h. The excitation wavelengths were (A) 514 nm excitation and (B) 785 nm. The inset shows the Raman microscope (50× magnification) image of the RGO sample (with three visible sheet edges) used for recording spectra. The films were obtained by drop casting 100 μL of the GO/RGO on a silicon wafer and allowing the sample to dry.

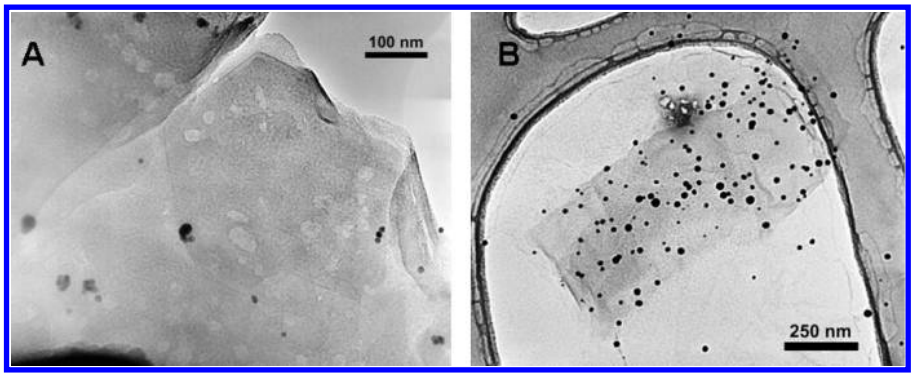

Figure 4. TEM micrograph of the RGO−Au composite at low resolution on a holey carbon grid. Panel A corresponds to the sequentially reduced sample, while panel B corresponds to the simultaneous reduction. The initial $HAuCl_4$ concentration used was 0.1 mM in both cases.

simultaneous reduction, the presence of the oxygenated functional groups on the GO surface are likely to provide binding sites for the $HAuCl_4$ and thus serve as nucleation sites for Au nanoparticles. The relatively slower reduction rate in the simultaneous reduction step further facilitates the growth of smaller size Au seeds into larger size particles. As shown earlier, any electrons stored in the RGO sheets can also contribute to the growth of metal nanoparticles. This variation in the particle size, dispersity, and density of the gold nanoparticles on the RGO surface highlights the merits of applying two procedures in bringing changes in the morphology of the composites.

The RGO−Au composites obtained from sequential and simultaneous reduction procedures are comprised of at least four sheets of variable lateral size stacked on top of each other. The TEM images at higher resolution (included in Supporting Information, Figure S1) provide lattice spacings of 2.04 and 2.36 Å, which correspond to the (200) and (111) faces of Au. The TEM images provide conclusive evidence that ultrasonic reduction at higher frequencies keeps RGO sheets intact, which serve as 2-D supports to anchor the metal particles. The Supporting Information also shows the TEM image of a single RGO sheet obtained by ultrasound reduction of GO at 20 kHz using a titanium horn (Figure S2). The micrograph clearly shows the damage caused by acoustic cavitation at 20 kHz. Whereas the 20 kHz probably leads to less stacking of the graphene sheets, the shear forces generated by using the Ti horn evidently cause substantial damage to the sheets.

We also wanted to probe whether the deposition of Au nanoparticles can influence the Raman bands of RGO itself. The Raman spectra of the RGO−Au composites at low Au concentration (0.1 mM) exhibited Raman bands similar to the one presented in Figure 3. The spectra of samples obtained from sequential and simultaneous reduction procedures using both 785 and 514 nm excitation are shown in Figure S3 (Supporting Information). A noticeable difference was seen when we increased the [Au]/[RGO] ratio. The Raman spectra (785 nm laser excitation) of RGO−Au composites at high gold concentrations are shown in Figure 5. At low concentrations of the gold (0.1 mM), the Raman spectra of the graphene bands remain unchanged as compared to the naked RGO surface (Figure S3, Supporting Information). However, upon increasing the gold concentration (1.5 mM), we observed a significant surface enhancement of the graphene Raman bands. The Raman spectra of bare RGO (curve a) and the surface-enhanced Raman spectra of the RGO−Au composite obtained by both sequential and simultaneous reduction (curves b and c) are included in Figure 5 for comparison. In the latter two cases, the laser power incident on the Au−RGO composites was reduced by 50% to avoid

DOI: 10.1021/jz1006093 | J. Phys. Chem. Lett. 2010, 1, 1987–1993

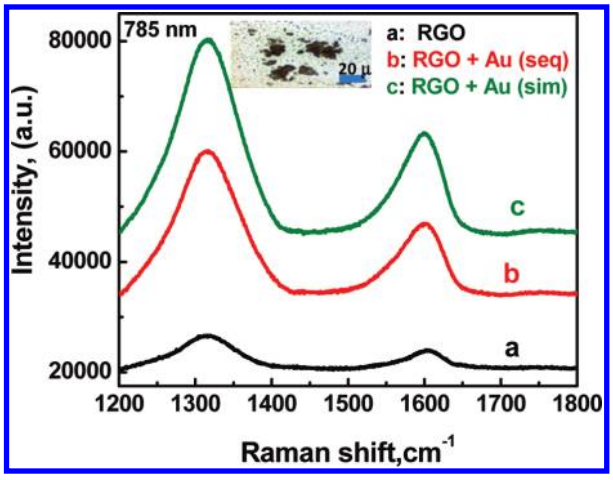

Figure 5. Raman spectra (785 nm laser excitation) of (a) 0.02% RGO in a 2% PEG solution. (b, c) Au−RGO composite samples (b) obtained from sequential reduction and (c) obtained after simultaneous reduction. The $HAuCl_4$ concentration used was 1.5 mM in both cases, with a total sonolysis time of 5 h to ensure complete reduction of the $HAuCl_4$. The GO concentration was the same as in that in (a). In both (b) and (c), the incident laser power was reduced by 50% to avoid saturation of the signal. The inset shows an example of the sampling spot (50× magnification) of the Au−RGO composite. The films were obtained by drop casting 100 μL of the appropriate sample on a silicon wafer and allowing the sample to dry.

saturation of the detector. Despite this reduction in laser power, the graphene peaks corresponding to both the D and G bands show a remarkable enhancement. The observed intensity enhancement is the same with both simultaneous and sequentially reduced Au−RGO samples. Although surface enhancements of the graphene peaks in the presence of gold nanoparticles have been attributed to chemical enhancements arising from the functional groups on the GO surface,[47] we consider that other effects can also play a role in the intensity enhancements. The dependence of the enhancement on the density of the gold nanoparticles on the RGO sheets indicates that electric field effects are also a contributing factor.

High-frequency ultrasound reduction is a convenient and clean approach to carry out reduction of GO using 2% PEG as a stabilizer. Both simultaneous and sequential reduction procedures can be adopted to obtain well-dispersed RGO−Au composites. The morphology of the RGO−Au nanocomposites varies depending on the reduction procedure employed. The enhanced Raman signals obtained with RGO−Au composites and their dependence on the gold concentration suggests a significant interaction between RGO and the gold particles. The ability of reduced graphene oxide to serve as a 2-D support to anchor metal nanoparticles is useful in developing next-generation sensors and energy conversion devices (fuel cells and storage batteries). Efforts are needed to exploit cooperative effects of the graphene and metal nanostructures for promoting catalytic processes.

EXPERIMENTAL METHODS

Ultrasound Operation. The solutions used for the ultrasonic reduction were made by mixing 0.02% GO and 0.1 mM tetrachloroauric acid, $HAuCl_4$, in a 2% aqueous solution of poly(ethylene glycol) (PEG, MW: 12000). The solutions were sonicated using an ultrasonic reactor (L-3 Communications, ELAC Nautik GMBH) operating at a frequency of 211 kHz. The sonication cell has a volume capacity of 200 mL, in which a 30 mL vial containing 20 mL of the graphene suspension was immersed in water. An argon atmosphere was maintained above the solution throughout the experiment. Sonication was carried out in continuous wave mode. A constant temperature of 293 K was maintained during the sonication by circulating cooling water through a jacket around the sonication cell. All sonication experiments were carried out at ultrasonic power between 110 and 125 mW/mL measured by calorimetry. This power was determined to be the optimum power setting based on the efficiency of sonochemical reduction in previous studies.[30,33] The sonication was stopped at various times, and absorption spectra were obtained using a 1 mm quartz cell on a Varian spectrophotometer (Cary Bio 50).

Raman Analysis. Raman spectra were acquired with Renishaw Raman microscope system using two different laser lines at 514.5 and 785 nm. The resolution was 4 cm^{-1}, and 180° backscattering geometry was employed using accumulation times of 100 and 10 s, respectively, for the 514.5 and 785 nm laser lines. The laser power directed through a 50× objective at the sample was < 1 mW at 514.5 nm and 3 mW at 785 nm. Spectral shift calibration was checked using the Raman lines for ethanol. All samples for Raman measurements were prepared by drop casting 10−100 μL of freshly prepared GO or RGO solutions on a silicon wafer and allowing the spot to dry.

TEM. The morphology and composition of the gold/RGO nanocomposites were characterized using a JEOL 2010 TEM outfitted with elemental analysis. Samples were drop cast onto holey carbon grids and dried under streaming N_2.

SUPPORTING INFORMATION AVAILABLE TEM image of RGO and Raman spectra of the RGO−Au composite. This material is available free of charge via the Internet at http://pubs.acs.org.

AUTHOR INFORMATION

Corresponding Author:

*To whom correspondence should be addressed. E-mail: kvinod@iun.edu (K.V.); masho@unimelb.edu.au (M.A.).

ACKNOWLEDGMENT We acknowledge the research support by the Australian Research Council (ARC). P.V.K. and I.L. acknowledge research funding by the Department of Energy, Office of Basic Energy Sciences. This is contribution number NDRL 4854 from the Notre Dame Radiation Laboratory

REFERENCES

(1) Wu, J.; Pisula, W.; Mullen, K. Graphenes as Potential Material for Electronics. *Chem. Rev.* **2007,** *107*, 718–747.
(2) Novoselov, K.; Geim, A. Graphene Detects Single Molecule of Toxic Gas. *Mater. Technol.* **2007,** *22*, 178–179.
(3) Seger, B.; Kamat, P. V. Electrocatalytically Active Graphene−Platinum Nanocomposites. Role of 2-D Carbon Support in PEM Fuel Cells. *J. Phys. Chem. C* **2009,** *113*, 7990–7995.

DOI: 10.1021/jz1006093 | *J. Phys. Chem. Lett.* **2010,** *1*, 1987–1993

(4) Stampfer, C.; Schurtenberger, E.; Molitor, F.; Guttinger, J.; Ihn, T.; Ensslin, K. Tunable Graphene Single Electron Transistor. *Nano Lett.* **2008,** *8*, 2378–2383.
(5) Rao, C. N. R.; Sood, A. K.; Voggu, R.; Subrahmanyam, K. S. Some Novel Attributes of Graphene. *J. Phys. Chem. Lett.* **2010,** *1*, 572–580.
(6) Cassagneau, T.; Fendler, J. H. High Density Rechargeable Lithium-Ion Batteries Self-Assembled from Graphite Oxide nanoplatelets and Polyelectrolytes. *Adv. Mater.* **1998,** *10*, 877–881.
(7) Yu, D.; Dai, L. Self-Assembled Graphene/Carbon Nanotube Hybrid Films for Supercapacitors. *J. Phys. Chem. Lett.* **2010,** *1*, 467–470.
(8) Liang, M. H.; Zhi, L. J. Graphene-Based Electrode Materials for Rechargeable Lithium Batteries. *J. Mater. Chem.* **2009,** *19*, 5871–5878.
(9) Pan, D. Y.; Wang, S.; Zhao, B.; Wu, M. H.; Zhang, H. J.; Wang, Y.; Jiao, Z. Li Storage Properties of Disordered Graphene Nanosheets. *Chem. Mater.* **2009,** *21*, 3136–3142.
(10) Paek, S. M.; Yoo, E.; Honma, I. Enhanced Cyclic Performance and Lithium Storage Capacity of SnO_2/Graphene Nanoporous Electrodes with Three-Dimensionally Delaminated Flexible Structure. *Nano Lett.* **2009,** *9*, 72–75.
(11) Kamat, P. V. Graphene-Based Nanoarchitectures. Anchoring Semiconductor and Metal Nanoparticles on a 2-Dimensional Carbon Support. *J. Phys. Chem. Lett.* **2010,** *1*, 520–527.
(12) Muszynski, R.; Seger, B.; Kamat, P. Decorating Graphene Sheets with Gold Nanoparticles. *J. Phys. Chem. C* **2008,** *112*, 5263–5266.
(13) Becerril, H. A.; Mao, J.; Liu, Z.; Stoltenberg, R. M.; Bao, Z.; Chen, Y. Evaluation of Solution-Processed Reduced Graphene Oxide Films as Transparent Conductors. *ACS Nano* **2008,** *2*, 463–470.
(14) Lightcap, I. V.; Kosel, T. H.; Kamat, P. V. Anchoring Semiconductor and Metal Nanoparticles on a 2-Dimensional Catalyst Mat. Storing and Shuttling Electrons with Reduced Graphene Oxide. *Nano Lett.* **2010,** *10*, 577–583.
(15) Williams, G.; Seger, B.; Kamat, P. V. TiO_2—Graphene Nanocomposites. UV-Assisted Photocatalytic Reduction of Graphene Oxide. *ACS Nano* **2008,** *2*, 1487–1491.
(16) Williams, G.; Kamat, P. V. Graphene—Semiconductor Nanocomposites. Excited-State Interactions between ZnO Nanoparticles and Graphene Oxide. *Langmuir* **2009,** *25*, 13869–13873.
(17) Ramesha, G. K.; Sampath, S. Electrochemical Reduction of Oriented Graphene Oxide Films: An in Situ Raman Spectroelectrochemical Study. *J. Phys. Chem. C* **2009,** *113*, 7985–7989.
(18) An, S. J.; Zhu, Y.; Lee, S. H.; Stoller, M. D.; Emilsson, T.; Park, S.; Velamakanni, A.; An, J.; Ruoff, R. S. Thin Film Fabrication and Simultaneous Anodic Reduction of Deposited Graphene Oxide Platelets by Electrophoretic Deposition. *J. Phys. Chem. Lett.* **2010,** *1*, 1259–1263.
(19) Ashokkumar, M.; Mason, T. Sonochemistry In *Kirk-Othmer Encylcopedia of Chemical Technology*; John Wiley & Sons: New York, 2007; pp 1—34.
(20) Hersam, M.; Green, A. Emerging Methods for Producing Monodisperse Graphene Dispersions. *J. Phys. Chem. Lett.* **2010,** *1*, 544–549.
(21) Buettner, J.; Gutierrez, M.; Henglein, A. Sonolysis of Water—Methanol Mixtures. *J. Phys. Chem.* **1991,** *95*, 1528–1530.
(22) Gutierrez, M.; Henglein, A.; Dohrmann, J. K. H Atom Reactions in The Sonolysis of Aqueous Solutions. *J. Phys. Chem.* **1987,** *91*, 6687–6690.
(23) Hart, E. J.; Henglein, A. Free Radical and Free Atom Reactions in The Sonolysis of Aqueous Iodide and Formate Solutions. *J. Phys. Chem.* **1985,** *89*, 4342–4347.
(24) Peller, J.; Wiest, O.; Kamat, P,V Sonolysis of 2,4-Dichlorophenoxyacetic Acid in Aqueous Solutions. Evidence for $^{\bullet}$OH-Radical-Mediated Degradation. *J. Phys. Chem. A* **2001,** *105*, 3176–3181.
(25) Stock, N. L.; Peller, J.; Vinodgopal, K.; Kamat, P. V. Combinative Sonolysis and Photocatalysis for Textile Dye Degradation. *Environ. Sci. Technol.* **2000,** *34*, 1747–1750.
(26) Caruso, R. A.; Ashokkumar, M.; Grieser, F. Sonochemical Formation of Gold Sols. *Langmuir* **2002,** *18*, 7831–7836.
(27) Gedanken., A. Using Sonochemistry for The Fabrication of Nanomaterials. *Ultrason. Sonochem.* **2004,** *11*, 47–55.
(28) He, Y.; Vinodgopal, K.; Ashokkumar, M.; Grieser, F. Sonochemical Synthesis of Ruthenium Nanoparticles. *Res. Chem. Intermed.* **2006,** *32*, 709–715.
(29) Maeda, Y.; Okitsu, K.; Inoue, H.; Nishimura, R.; Mizukoshi, Y.; Nakui, H. Preparation of Nanoparticles by Reducing Intermediate Radicals Formed in Sonolytical Pyrolysis of Surfactants. *Res. Chem. Intermed.* **2004,** *30*, 775–783.
(30) Okitsu, K.; Ashokkumar, M.; Grieser, F. Sonochemical Synthesis of Gold Nanoparticles: Effects of Ultrasound Frequency. *J. Phys. Chem. B* **2005,** *109*, 20673–20675.
(31) Mizukoshi, Y.; Okitsu, K.; Y, M.; Yamamoto, T.; Oshima, R.; Nagata, Y. Sonochemical Preparation of Bimetallic Nanoparticles of Gold/Palladium in Aqueous Solutions. *J. Phys. Chem. B* **1997,** *101*, 7033–7037.
(32) Jia, Y.; Niu, H.; Wu, M.; Ning, M.; Zhu, H.; Chen, Q. Sonochemical Preparation of Bimetallic Co/Cu Nanoparticles in Aqueous Solutions. *Mater. Res. Bull.* **2005,** *40*, 1623–1629.
(33) Vinodgopal, K.; He, Y.; Ashokkumar, M.; Grieser, F. Sonochemically Prepared Platinum—Ruthenium Bimetallic Nanoparticles. *J. Phys. Chem. B* **2006,** *110*, 3849–3852.
(34) Kan, C.; Cai, W.; Li, C.; Zhang, L.; Hofmeister, H. Ultrasonic Synthesis and Optical Properties of Au/Pd Bimetallic Nanoparticles in Ethylene Glycol. *J. Phys. D: Appl. Phys.* **2003,** *36*, 1609–1614.
(35) Mizukoshi, Y.; Okitsu, K.; Maeda, Y.; Yamamoto, T. A.; Oshima, R.; Nagata, Y. Sonochemical Preparation of Bimetallic Nanoparticles of Gold/Palladium in Aqueous Solution. *J. Phys. Chem. B* **1997,** *101*, 7033–7037.
(36) Mizukoshi, Y.; Fujimoto, T.; Nagata, Y.; Oshima, R.; Maeda, Y. Characterization and Catalytic Activity of Core—Shell Structured Gold/Palladium Bimetallic Nanoparticles Synthesized by Sonochemical Method. *J. Phys. Chem. B* **2000,** *104*, 6028–6032.
(37) Hung, H. M.; Hoffmann, M. R. Kinetics and Mechanism of The Sonolytic Degradation of Chlorinated Hydrocarbons: Frequency Effects. *J. Phys. Chem. A* **1999,** *103*, 2734–2739.
(38) Okitsu, K.; Sharyo, K.; Nishimura, R. One-Pot Synthesis of Gold Nanorods by Ultrasonic Irradiation: The Effect of pH on The Shape of The Gold Nanorods and Nanoparticles. *Langmuir* **2009,** *25*, 7786–7790.
(39) Suslick, K. S.; Price, G. J. Applications of Ultrasound to Materials Chemistry. *Annu. Rev. Mater. Sci.* **1996,** *29*, 295–326.
(40) Ciawi, E.; Rae, J.; Ashokkumar, M.; Grieser, F. Determination of Temperatures Within Acoustically Generated Bubbles in Aqueous Solutions at Different Ultrasound Frequencies. *J. Phys. Chem. B* **2006,** *110*, 13656–13660.
(41) Rae, J.; Ashokkumar, M.; Eulaerts, O.; von Sonntag, C.; Reisse, J.; Grieser, F. Estimation of Ultrasound Induced Cavitation Bubble Temperatures in Aqueous Solutions. *Ultrason. Sonochem.* **2005,** *12*, 325–329.

DOI: 10.1021/jz1006093 | *J. Phys. Chem. Lett.* **2010,** *1*, 1987–1993

(42) Gutierrez, M.; Henglein, A.; Dohrmann, J. K. H Atom Reactions in the Sonolysis of Aqueous-Solutions. *J. Phys. Chem.* **1987,** *91*, 6687–6690.
(43) Tauber, A.; Mark, G.; Schuchmann, H.-P.; von Sonntag, C. Sonolysis of Tert-butyl-Alcohol in Aqueous Solution. *Perkin Trans. 2* **1999,** 1129–1135.
(44) Gutierrez, M.; Henglein, A.; Ibanez, F. Radical Scavenging in The Sonolysis of Aqueous Solutions of I^-, Br^-, and N_3^-. *J. Phys. Chem.* **1991,** *95*, 6044–6047.
(45) Kamat, P. V.; Vinodgopal, K. Sonochromic Effect in WO_3 Colloidal Suspensions. *Langmuir* **1996,** *12*, 5739–5741.
(46) Cassagneau, T.; Fendler, J. H. Preparation and Layer-by-Layer Self-Assembly of Silver Nanoparticles Capped by Graphite Oxide Nanosheets. *J. Phys. Chem. B* **1999,** *103*, 1789–1793.
(47) Jasuja, K.; Berry, V. Implantation and Growth of Dendritic Gold Nanostructures on Graphene Derivatives: Electrical Property Tailoring and Raman Enhancement. *ACS Nano* **2009,** *3*, 2358–2366.

DOI: 10.1021/jz1006093 | *J. Phys. Chem. Lett.* **2010,** *1*, 1987–1993